SLAC-PUB-15433

Submitted to *The Astrophysical Journal*

Fermi Large Area Telescope Observations of the Active Galaxy 4C +55.17: Steady, Hard Gamma-Ray Emission and its Implications

W. McConville[1,2,3], L. Ostorero[4,5,6,7] R. Moderski[8], Ł. Stawarz[9,10,11] C. C. Cheung[12,13], M. Ajello[14], A. Bouvier[15] J. Bregeon[16], D. Donato[17,2], J. Finke[18], A. Furniss[19] J. E. McEnery[1,2], M. E. Monzani[14], M. Orienti[20,21], L. C. Reyes[22], A. Rossetti[21], D. A. Williams[19]

[1]NASA Goddard Space Flight Center, Greenbelt, MD 20771, USA

[2]Department of Physics and Department of Astronomy, University of Maryland, College Park, MD 20742, USA

[3]email: wmcconvi@umd.edu

[4]Dipartimento di Fisica Generale "Amedeo Avogadro", Università degli Studi di Torino, Via P. Giuria 1, I-10125 Torino, Italy

[5]Istituto Nazionale di Fisica Nucleare (INFN), Sezione di Torino, Via P. Giuria 1, I-10125 Torino, Italy

[6]Department of Physics & Astronomy, University of Pennsylvania, 209 S. 33rd St., Philadelphia, PA 19104, USA

[7]Harvard-Smithsonian Center for Astrophysics, 60 Garden Street, Cambridge, MA 02138, USA

[8]Nicolaus Copernicus Astronomical Center, ul. Bartycka 18, 00-716 Warsaw, Poland

[9]Institute of Space and Astronautical Science, JAXA, 3-1-1 Yoshinodai, Chuo-ku, Sagamihara, Kanagawa 252-5210, Japan

[10]Astronomical Observatory, Jagiellonian University, 30-244 Kraków, Poland

[11]email: stawarz@astro.isas.jaxa.jp

[12]National Research Council Research Associate, National Academy of Sciences, Washington, DC 20001, resident at Naval Research Laboratory, Washington, DC 20375, USA

[13]email: Teddy.Cheung.ctr@nrl.navy.mil

[14]W. W. Hansen Experimental Physics Laboratory, Kavli Institute for Particle Astrophysics and Cosmology, Department of Physics and SLAC National Accelerator Laboratory, Stanford University, Stanford, CA 94305, USA

[15]Santa Cruz Institute for Particle Physics, Department of Physics and Department of Astronomy and Astrophysics, University of California at Santa Cruz, Santa Cruz, CA 95064, USA

[16]Istituto Nazionale di Fisica Nucleare, Sezione di Pisa, I-56127 Pisa, Italy

[17]Center for Research and Exploration in Space Science and Technology (CRESST) and NASA Goddard Space Flight Center, Greenbelt, MD 20771, USA

[18]Space Science Division, Naval Research Laboratory, Washington, DC 20375, USA

[19]Santa Cruz Institute for Particle Physics and Department of Physics, University of California, Santa Cruz, CA 95064, USA

[20]Dipartimento di Astronomia, Università di Bologna, via Ranzani 1, I-40127, Bologna, Italy

[21]Istituto di Radioastronomia INAF, via Gobetti 101, 40129 Bologna, Italy

[22]Kavli Institute for Cosmological Physics, University of Chicago, Chicago, IL 60637, USA

Published in Astrophys.J.738:148,2011 and arXiv:1107.1471.

Work supported in part by US Department of Energy under contract DE-AC02-76SF00515.

ABSTRACT

We report *Fermi*/LAT observations and broad-band spectral modeling of the radio-loud active galaxy 4C +55.17 (z=0.896), formally classified as a flat-spectrum radio quasar. Using 19 months of all-sky survey *Fermi*/LAT data, we detect a γ-ray continuum extending up to an observed energy of 145 GeV, and furthermore we find no evidence of γ-ray variability in the source over its observed history. We illustrate the implications of these results in two different domains. First, we investigate the origin of the steady γ-ray emission, where we re-examine the common classification of 4C +55.17 as a quasar-hosted blazar and consider instead its possible nature as a young radio source. We analyze and compare constraints on the source physical parameters in both blazar and young radio source scenarios by means of a detailed multiwavelength analysis and theoretical modeling of its broad-band spectrum. Secondly, we show that the γ-ray spectrum may be formally extrapolated into the very-high energy (VHE; $\geq 100\,\mathrm{GeV}$) range at a flux level detectable by the current generation of ground-based Cherenkov telescopes. This enables us to place constraints on models of extragalactic background light (EBL) within LAT energies and features the source as a promising candidate for VHE studies of the Universe at an unprecedented redshift of z=0.896.

Subject headings: galaxies: active — galaxies: individual (4C +55.17) — galaxies: jets — gamma rays: observations — radiation mechanisms: non-thermal

1. Introduction

The radio-loud active galaxy 4C +55.17 (0954+556), formally classified as a flat spectrum radio quasar (FSRQ), has a history of γ-ray observations dating back to the EGRET era, as 3EG J0952+5501 (Hartman et al. 1999; Mattox et al. 2001) and EGR J0957+5513 (Casandjian & Grenier 2008). Due to a relatively poor localization of the EGRET source, however, the association of the γ-ray emitter with 4C +55.17 remained tentative at that time. After the successful launch of the *Fermi* Gamma-Ray Space Telescope in June 2008, this association was on the other hand quickly confirmed by the Large Area Telescope (LAT; Atwood et al. 2009), initially as 0FGL J0957.6+5522 (Abdo et al. 2009a,b), and most recently as 1FGL J0957.7+5523 (Abdo et al. 2010a).

The quasar classification of 4C +55.17 may be attributed to the presence of broad optical emission lines in its spectrum (Wills et al. 1995) and high optical/UV core luminosity (absolute B-band magnitude, $M_\mathrm{B} < -23$; Veron-Cetty & Veron 2006). Its redshift[23], $z = 0.896$, is based on the detection of Lyα and CIV lines with the HST-FOS (Wills et al. 1995) and Mg II in the SDSS

[23]Assuming a ΛCDM cosmology with $H_0 = 71\,\mathrm{km\,s^{-1}\,Mpc^{-1}}$, $\Omega_\mathrm{M} = 0.27$, and $\Omega_\Lambda = 0.73$, the luminosity distance $d_\mathrm{L} = 5785\,\mathrm{Mpc}$, and the conversion scale is $1\,\mathrm{mas} = 7.8\,\mathrm{pc}$.

spectrum (Schneider et al. 2007). The optical-UV properties of the source, together with its high γ-ray luminosity of the order $L_\gamma \simeq 10^{47}\,\mathrm{erg\,s^{-1}}$, have in turn led to the common classification of 4C +55.17 as a blazar/FSRQ.

However, 4C +55.17 also exhibits a number of morphological and spectral properties that have placed its exact blazar/FSRQ classification into question (Marscher et al. 2002; Rossetti et al. 2005). FSRQs are uniquely characterized by the presence of a central compact radio core exhibiting a highly variable flat-spectrum continuum, high brightness temperatures (T_b), and, typically, superluminal motions on VLBI scales (Urry & Padovani 1995). Indeed, all of the aforementioned radio properties are shared by the luminous blazars detected in γ-rays: these are exclusively observed to possess compact, highly polarized jets a few milli-arcseconds (mas) in angular size, and unresolved radio cores with brightness temperatures in the range $T_\mathrm{b} = 10^{10} - 10^{14}\,\mathrm{K}$ when observed at 5 GHz (Taylor et al. 2007) and 15 GHz (Kovalev et al. 2009). In comparison, 4C +55.17 demonstrates none of these characteristics. To date, the source shows no evidence of blazar flaring at any wavelength, nor any evidence of long-term variability, with the exception of a $\sim 30\%$ optical flux-density change noted over a period of 7 years between recent *Swift*/UVOT measurements and archival SDSS data (see § 2.2 and § 3.1 for discussion). Furthermore, the VLBI radio morphology of the source is extended over $\sim 400\,\mathrm{pc}$ (projected). The peak surface brightness in a VLBA 15 GHz image taken from Rossetti et al. (2005) is found in the northernmost component and is clearly resolved, with a corresponding brightness temperature $T_\mathrm{b} < 2 \times 10^8$ K (consistent with a measurement at 5 GHz; Taylor et al. 2007), which is uncharacteristic of all the other known quasar-hosted γ-ray blazars.

Based on the radio morphology of 4C +55.17, Rossetti et al. (2005) first suggested that the source may in fact belong to the family of young radio sources (for a review, see O'Dea 1998), rather than blazars. Such sources are characterized by a very low radio variability (if any) and symmetric double radio structures resembling "classical doubles" on much smaller scales: linear sizes $\lesssim 1\,\mathrm{kpc}$ for compact symmetric objects (CSOs) and $\sim 1 - 15\,\mathrm{kpc}$ for medium symmetric objects (MSOs; Augusto et al. 2006), to be compared with the typical linear sizes of "regular" Fanaroff-Riley type-II radio galaxies of $\sim 100\,\mathrm{kpc}$. In many cases, CSO sources are found to exhibit a turnover in their radio spectra in the range of 0.5−10 GHz, as the so-called Gigahertz Peaked Spectrum (GPS) objects do (de Vries et al. 1997); similarly, MSO's often display turnover frequencies below 0.5 GHz, typical of the Compact Steep Spectrum (CSS) class of sources (Fanti et al. 1990). The overlap between CSO and GPS samples, as well as between samples of MSOs and CSS sources, is however not complete (Snellen et al. 2000; Augusto et al. 2006). In the case of 4C +55.17, the VLBI morphology at 5 GHz reveals two distinct emission regions, to the north and south (Rossetti et al. 2005, see also Figure 1), covering a total angular extent of 53 mas (= 413 pc, projected). On the kpc scale, the source reaches $4''.5$ ($\sim 35\,\mathrm{kpc}$, projected), and it is resolved with the VLA in three components, the central one hosting the VLBI structure. The northern component of the pc-scale emission features a compact region with a relatively flat spectrum ($\alpha = 0.4; F_\nu \propto \nu^{-\alpha}$; Rossetti et al. 2005), which can be attributed to a core or a hotspot region, while the southern component features a more diffuse and

slightly steeper-spectrum ($\alpha = 0.49$) region. Rossetti et al. (2005) have pointed out that these two components resemble more compact hotspots and lobes, suggesting a CSO/MSO classification for this object. The kpc-scale emission might thus be interpreted as a remnant of previous jet activity, as this is a common feature among sources that show evidence of intermittent behavior (e.g., Baum et al. 1990; Luo et al. 2007; Orienti & Dallacasa 2008). Under the CSO/MSO framework, Rossetti et al. found no core candidate between the VLBA-scale lobes at a level $\gtrsim 2$ mJy/beam in a 15 GHz map.

An 11-month comparison of the γ-ray variability and spectral properties of 4C +55.17 against the other LAT FSRQs highlights the unusual nature of the source (Abdo et al. 2010a,b). Among all of the sources originally detected in the 3-month LAT Bright AGN Sample (LBAS; Abdo et al. 2009b) that were classified as FSRQs, 4C +55.17 is characterized by the lowest variability index (Abdo et al. 2010a). In addition, the unusually hard γ-ray continuum (that is, with a low photon index Γ) is found to be one of the hardest among FSRQs in the 1st LAT AGN Catalog (1LAC; Abdo et al. 2010b). In fact, of those sources included in the 1LAC (FSRQ or otherwise) with > 1 GeV flux greater than or equal to that of 4C +55.17, only five – all of which are BL Lac objects (PKS 2155–304, Mkn 421, 3C 66A, PG 1553+113, and PKS 0447-439) – appear with a harder γ-ray spectrum.

In this work, we re-examine the high-energy γ-ray (> 100 MeV) properties of 4C +55.17 using 19 months of LAT all-sky survey data and discuss the implications of these results in two domains. First, we reconsider the underlying physical processes responsible for the γ-ray emission through detailed broadband modeling of the source in the context of two scenarios: "young radio source" and "blazar." In addition, we demonstrate that the unusual properties of the source make it an ideal candidate for studying the high-redshift universe at very-high energies (VHE), in particular for placing constraints on the level of extragalactic background light (EBL). The paper is organized as follows. Section 2 details the analysis of 19 months of LAT data and discusses the supporting multiwavelength observations. In particular, section 2.1 focuses on the LAT data reduction, presenting new spatial (localization), spectral, and variability analysis, including a detailed analysis of the 145 GeV photon detection associated with the source (see also Appendix A). Section 2.2 discusses the multiwavelength observations, including analysis of archival radio and *Swift* X-ray and optical data, as well as a new hard X-ray detection with the *Swift* Burst Alert Telescope (BAT). Spectral properties and classification of 4C +55.17 are discussed in section 3. We follow with a detailed analysis of the high energy spectrum of 4C +55.17, where we place constraints on models of EBL and discuss the implications of the 145 GeV photon detection to future VHE observations of the source (§ 3.2). Our conclusions are presented in section 4.

2. Observations

2.1. *Fermi*/LAT Observations

The *Fermi*/LAT is a pair creation telescope designed to cover the energy range from $\sim 20\,\mathrm{MeV}$ to $> 300\,\mathrm{GeV}$ (Atwood et al. 2009). The LAT instrument features an improved angular resolution ($\theta_{68\%} = 0.8^\circ$ at 1 GeV) over previous instruments and a large field-of-view of 2.4 sr. The nominal mode of operation is an all-sky survey mode, which provides nearly uniform sky coverage approximately every 3 hours. The following analysis is comprised of 19 months of nominal all-sky survey data extracted from a 10° region of interest (ROI) around the J2000.0 radio position of 4C +55.17 (R.A. = $09^{\mathrm{h}}57^{\mathrm{m}}38.1844^{\mathrm{s}}$, Decl. = $55^\circ22'57.769''$; Fey et al. 2004) and covers the mission elapsed time (MET) 239557417 to 289440000 (August 4, 2008 through March 4, 2010). A 100-second interval at MET 251059717 was removed in order to avoid contamination from GRB 081215A, which fell within the ROI. Event selections include the "diffuse" event class (Atwood et al. 2009) recommended for point source analysis, a zenith angle cut of $< 105^\circ$ to avoid contamination from the earth limb, and rocking angle cuts at 43° and 52°, respectively, for times corresponding to a change in the instrument's rocking angle from 39° to 50° that occured on September 3, 2009 (MET 273628805). Science Tools `v9r16p1` and instrument response functions (IRFs) `P6_V3_DIFFUSE` were used for this analysis.

The 19 month LAT localization of 4C +55.17 was determined using `gtfindsrc`, resulting in a best-fit position (J2000.0) of R.A. = $09^{\mathrm{h}}57^{\mathrm{m}}40^{\mathrm{s}}$, Decl. = $55^\circ23'40''$, which is $0.012^\circ = 0.7'$ offset from the radio position and falls within the 95% error circle $r_{95\%} = 0.017^\circ = 1.0'$ (statistical only). In order to model the γ-ray emission, all point sources from the 1FGL catalog (Abdo et al. 2010a) within 15° of the source were included. Sources within 10° of the 4C +55.17 radio position were modeled with their flux and spectral parameters set free, while those sources that fell outside the 10° ROI were fixed at their catalog values. The diffuse background was modelled using the recommended[24] Galactic diffuse `gll_iem_v02.fit` along with the corresponding isotropic spectral template `isotropic_iem_v02.txt`.

Prior to fitting the spectrum, the high energy photons attributable to the 4C +55.17 position (both radio and γ-ray) were found by comparing the energy and incoming angle θ (defined with respect to the spacecraft zenith) of each photon within the ROI to the 95% containment radius of the point spread function defined by the `P6_V3_DIFFUSE` IRFs. Included among those photons was a 145 GeV event at an angular separation of 0.06° (R.A. = $09^{\mathrm{h}}58^{\mathrm{m}}03^{\mathrm{s}}$, Decl. =$55^\circ24'00''$) from the 4C +55.17 position, falling well within the 95% containment radius for the given energy and angle of incidence. Through an analysis of the event diagnostics, the photon nature of this event is confirmed here for the first time (for further details regarding the 145 GeV event analysis, see Appendix A). In addition, several photons in the $\sim 30 - 55$ GeV range were also detected. The association of the 145 GeV photon with 4C +55.17 tentatively places it as the highest-redshift source

[24] `http://fermi.gsfc.nasa.gov/ssc/data/access/lat/BackgroundModels.html`

to be observed at VHE to date.

A spectral analysis of 4C +55.17 was performed with `gtlike` using the LAT data between 100 MeV and 300 GeV. Spectral data points were first obtained by fitting each of 9 equal logarithmically spaced energy bins to a separate power law with index and prefactor parameters set free. From the resulting data points, a break in the spectrum could be seen to occur at ~ 1.6 GeV. This was confirmed by performing an independent unbinned likelihood fit over all the data from 100 MeV to 20 GeV using power law, log parabola, and broken power law models, with the break energy of the broken power law fixed at the peak in the νF_ν representation ($E_{\rm br} \sim 1.6$ GeV). The maximum energy of 20 GeV was chosen in order to avoid fitting any portion of the spectrum that may be significantly attenuated by the EBL. A likelihood ratio test (Mattox et al. 1996) resulted in a 4.1σ improvement of the broken power law over the single power law used in previous analyses of the source (Abdo et al. 2009a, 2010a), as compared to a 3.8σ improvement over the power law from the log parabola. We therefore consider the broken power law to be the most accurate representation of the intrinsic γ-ray spectrum of the source.

To test the γ-ray variability over the 19-month period, we made light curves in time bins of 7 and 28 days. Due to the limited statistics over each interval, the source was fit to a single power-law in each bin, with index and prefactor parameters free. To improve the fit convergence, point sources in the ROI were included only if they were detected with a test statistic (TS; Mattox et al. 1996) greater than 1 ($\sim 1\sigma$). The resulting light curve (> 100 MeV), divided into 7 day bins, is shown in Figure 2. The variability of 4C +55.17 was analyzed by means of a χ^2 test, where we assumed the model describing the data to be a constant straight line with intercept equal to the weighted mean of all $> 3\sigma$ detections. This test yielded a χ^2 probability $P(\chi^2 \geq \chi^2_{\rm obs})$ of 0.96 and 0.87 for the 7 day and 28 day light curves, respectively, and was thus in agreement with the tested hypothesis. We therefore found no evidence of variability in γ-rays over the 19-month LAT observing period, consistent with the previous 11-month lightcurve analysis ($\sim$ 30 day bins) from Abdo et al. (2010a). In addition, the weighted mean for this period was found to be $(9.5 \pm 0.4_{\rm stat} + 0.83_{\rm sys} - 0.49_{\rm sys}) \times 10^{-8}\,{\rm ph\,cm^{-2}\,s^{-1}}$, which is consistent with the EGRET measured flux of $(9.1 \pm 1.6) \times 10^{-8}\,{\rm ph\,cm^{-2}\,s^{-1}}$ (Hartman et al. 1999) as well. Systematic uncertainties on the LAT flux were determined by bracketing the instrument effective area to values of 10%, 5%, and 20% their nominal values at $\log({\rm E/MeV}) = 2, 2.75$, and 4, respectively. We note that these findings differ from those of Neronov et al. (2010), who claim variability between the EGRET and LAT measured fluxes. We believe this discrepancy lies in a mis-quoted value of the EGRET flux.

2.2. Multiwavelength Data

2.2.1. X-ray

We analyzed all *Swift* (Gehrels et al. 2004) data obtained over the 19-month LAT observing period, which consisted of three X-ray Telescope (XRT; Burrows et al. 2005) snapshots (1.6-4.5 ks),

in order to check the X-ray state of the source. We used the xrtgrblc script (available in the HEASoft package version 6.8) to analyze the XRT observations: we reprocessed the data stored in the HEASARC archive using the latest XRT calibration database (20091130), selecting the events with 0-12 grades in photon counting mode (PC). The scripts chose the optimal source and background extraction regions based on the source intensity: the X-ray photons were extracted using a $25''$ circle for the source and an annulus with $50'' - 150''$ inner-outer radius for the background. Adding all of the exposure and performing a C-statistic fit from $0.3 - 10\,\mathrm{keV}$ using XSpec12, we found the best fit obtained to be a power law with absorption fixed at the galactic value ($N_{\mathrm{H}} = 9 \times 10^{19}\,\mathrm{cm}^{-2}$), where we obtained the photon index $\Gamma = 1.84 \pm 0.19$, with an absorbed flux of $(8.3^{+1.7}_{-1.4}) \times 10^{-13}\,\mathrm{erg\,cm^{-2}\,s^{-1}}$ and an unabsorbed flux of $(8.5^{+1.7}_{-1.4}) \times 10^{-13}\,\mathrm{erg\,cm^{-2}\,s^{-1}}$. Comparing each of the individual observations, no X-ray variability was found, with all measurements falling within the joint errors. These results were also compared with previous *Chandra* data (Tavecchio et al. 2007) obtained June 16, 2004, where the flux was found again to be non-variable within the statistical errors. Finally, historical X-ray data from ROSAT (Comastri et al. 1997) obtained November 7, 1993 were included in the spectral energy distribution (SED) modeling to further constrain the soft X-ray portion of the spectrum.

In the hard X-rays, data from the *Swift*/BAT (Ajello et al. 2008, 2009) were analyzed using five years of cumulative exposure from November $2005 - 2010$. We detect the source for the first time in the hard X-ray band, with a $15 - 150\,\mathrm{keV}$ flux of $(6.75^{+0.38}_{-5.21}) \times 10^{-12}\,\mathrm{erg\,cm^{-2}\,s^{-1}}$ and a power-law photon index, $\Gamma = 1.79^{+1.17}_{-0.84}$.

2.2.2. Optical & Infrared

During each of the three *Swift* pointings in 2009, Ultra-Violet/Optical Telescope (UVOT; Roming et al. 2005) observations were also obtained. Data were obtained in all 6 filters in the first two epochs, and the last epoch with only the $W2$ filter. The data reduction and analysis was performed using the uvotgrblc script, which reprocesses the data stored in the HEASARC using the latest UVOT calibration database (20100129). The optimal source and background extraction regions were a $5''$ circle and a $27'' - 35''$ annulus, respectively. Table 1 summarizes these observations. A comparison of the results between each epoch shows the source to fall within the joint errors in flux in the optical to UV bands across all three epochs. These results were also compared with archival SDSS data from February 2, 2002 (Adelman-McCarthy et al. 2008). A comparison of the UVOT and SDSS U-band flux densities shows an increase from $(0.187 \pm 0.003)\,\mathrm{mJy}$ in the SDSS data to $(0.250 \pm 0.007)\,\mathrm{mJy}$ in the UVOT data, indicating a $\sim 30\%$ rise in flux over 7 years. In addition, the UVOT V- and B-band flux densities were averaged using a least-squares approach to a linear fit and compared with the SDSS g-band, which fell between the two. The average of the UVOT V- and B-bands, measured at $(0.305 \pm 0.014)\,\mathrm{mJy}$, shows a similar $\sim 25\%$ increase from the SDSS measured value of $(0.240 \pm 0.011)\,\mathrm{mJy}$. A comparison of the *Swift* UVOT measurements to the continuum flux underlying the Lyα line obtained by HST-FOS in 1993 (Wills et al. 1995)

shows the fluxes to be equal between these two periods.

In the near-infrared, we included historical data from the 2MASS Point Source Catalog (Cutri et al. 2003), for which the absolute calibration was taken from Cohen et al. (2003). All infrared, optical, and ultraviolet data were dereddened by means of the extinction laws given by Cardelli et al. (1989), assuming a B-band Galactic extinction ($A_{\rm B} = 0.038$) as determined via Schlegel et al. (1998), and a ratio of total to selective absorption at V equal to $R_{\rm V} = 3.09$ (Rieke & Lebofsky 1985).

2.2.3. Radio

To model the γ-ray emission in 4C+55.17 (sec. 3.1), we compiled integrated radio to sub-mm measurements of the source (Bloom et al. 1994; Huang et al. 1998; Reich et al. 1998; Jenness et al. 2010), including 5-year WMAP data (Wright et al. 2009), and other archival data from the NASA/IPAC Extragalactic Database (NED). In order to isolate the total radio flux from the inner ~ 400 pc scale structure[25], we re-analyzed several archival VLA data sets from 5 to 43 GHz (see Figures 3 and 4). The typical resolutions are $\sim 0.1''$ to $0.4''$, ensuring a total measurement of the ~ 50 mas scale structure without loss of flux as in the VLBI observations (e.g., Rossetti et al. 2005). We also include similar measurements from previously published VLA 5 and 8.4 GHz (Reid et al. 1995; Myers et al. 2003; Tavecchio et al. 2007) and MERLIN 0.4 and 1.7 GHz (Reid et al. 1995) maps.

The radio variability properties of 4C +55.17 are important for assessing its nature. We therefore searched the literature for various archival radio to sub-mm monitoring observations of the source (e.g. Altschuler & Wardle 1976; Wardle et al. 1981; Seielstad et al. 1983; Jenness et al. 2010), including 22 and 37 GHz data from the Metsähovi monitoring program (Teräsranta et al. 1998, 2004, 2005). While the Wardle et al. (1981) data was not directly available, we note from the literature that the authors found the source to be non-variable. Variability in each of the remaining cases was measured by applying a statistical χ^2 test of the available data using the hypothesis of a constant source with flux equal to the weighted mean. The results were consistent with the tested hypothesis in each case, with the exception of the Metsähovi data, which yielded probabilities $\mathrm{P}(\chi^2 \geq \chi^2_{\rm obs})$ of 6.44×10^{-56} and 8.56×10^{-24} at 22 GHz and 37 GHz, respectively. To quantify this variability, we compared fractional variability indices using the formula $\mathrm{Var}_{\Delta \rm S} = (\mathrm{S}_{\rm max} - \mathrm{S}_{\rm min})/\mathrm{S}_{\rm min}$ used in a variability study of GPS sources (Torniainen et al. 2007), where we obtained values of 3.5 and 1.43 at 22 and 37 GHz, respectively. The 22 GHz value fell slightly above the nominal variability threshold of 3.0 set by Torniainen et al. (2007) as an upper limit for the bona fide GPS sources. This result, however, arose due to a single outlying flux measurement at 22 GHz of 0.32 ± 0.09 Jy which occurred ~ 40 minutes after a previous measurement of 1.12 ± 0.08 Jy at the

[25]The kpc-scale radio emission is not expected to contribute significantly toward the modeling of the high energy portion of the spectrum (see §3.1.1 & §3.1.2).

same frequency[26]. Removing this questionable flux point and performing the test again resulted in a fractional variability index of 0.89, which fell well within the proposed threshold for genuine GPS galaxies. We therefore find the degree of variability in 4C +55.17 to be consistent with the behavior of confirmed young radio galaxies, rather than blazars.

3. Results

3.1. Modeling & Classification

3.1.1. CSO Modeling

As noted in the introduction, there are several reasons to consider the possible nature of 4C +55.17 as an example of a luminous AGN exhibiting recurrent jet activity, with young and symmetric (CSO-type) inner radio structure instead of a "core-jet" morphology typical of blazars. While the physical nature and the origin of the CSOs is at some level still debated, the most likely and widely accepted hypothesis states that they are the young versions of present-day extended radio galaxies (Philips & Mutel 1982; Fanti et al. 1995). In the alternative explanation, these sources are considered to be of a similar age to normal radio galaxies, but only confined/frustrated due to dramatic interactions with a surrounding dense gas in their host galaxies (van Breugel et al. 1984; Wilkinson et al. 1994). The latter scenario is however inconsistent with the lack of observational evidence for the amount of ambient gas required to supply sufficient confinement (De Young 1993; Carvalho 1994, 1998; Siemiginowska et al. 2005; see, however, Garcia-Burillo et al. 2007 for notable exceptions). More promising is therefore the "youth" scenario for CSOs, for which a number of evolutionary models were proposed (Begelman 1996; De Young 1997; Perucho & Marti 2002; Kawakatu & Kino 2006).

While many observational properties of 4C +55.17 make its classification as a young radio source compelling, it is also worth noting the characteristics that could make such a classification potentially difficult. For example, if 4C +55.17 is indeed a CSO, it is the only such object to be identified as a γ-ray emitter in 1FGL/1LAC, with a GeV flux nearly an order of magnitude higher than the lower limit of the complete flux-limited subsample within the 1LAC catalog (Abdo et al. 2010b). This would immediately set the object apart as an outstanding member of its class. In addition, the relatively high radio polarization of the source ($\sim 3\%$ in a $\sim 0.2''$ resolution VLA 8.4 GHz image; Jackson et al. 2007), is uncharacteristic of the typically low ($< 1\%$) radio polarization seen among CSOs (Readhead et al. 1996), although polarized emission from CSOs has occasionally been found (e.g., Gugliucci et al. 2007). The low polarization of CSOs, which are entirely embedded within the inner regions of the host galaxy, is often attributed to the large expected Faraday depths of

[26]Variability within hour timescales is rare at the frequencies observed by Metsähovi (A. Lahteenmaki, T. Hovatta, & M. Tornikoski, private communication 2010)

the surrounding interstellar medium (Burn 1966; Bicknell et al. 1997; Gugliucci et al. 2007). The surrounding medium may also play a key role in shaping the spectral turnover seen in the GPS class of young radio sources, through the free-free absorption (FFA) process (either internal or external to the emission region; Bicknell et al. 1997; Begelman 1999; Peck et al. 1999). The nature of the absorber is however still widely debated, and both the synchrotron self-absorption (SSA) and FFA processes are considered as viable options (O'Dea & Baum 1997; Snellen et al. 2000).

If FFA effects are indeed responsible for the spectral turnover in GPS sources, then the relatively flat ($\alpha \simeq 0.4 - 0.5$) power-law radio continuum of 4C +55.17, which shows no indication of a low-energy turnover, may indicate an exceptionally small amount of ionized ambient gas in the vicinity of its young radio structure. More specifically, if the radio absorber may be identified with ionization-bounded hydrogen clouds of interstellar matter present at pc to kpc distances from the center and engulfed by the expanding lobes, as proposed by Begelman (1999) and advocated by Stawarz et al. (2008), and if a significant part of this gas has been evacuated prior the onset of new jet activity, then one would expect much less severe absorption of the low frequency radio emission, resulting in a lower turnover frequency compared to that of GPS galaxies. In this case, the relatively high polarization of 4C +55.17 (as for a young radio source) would find a natural and straightforward explanation as well.

In considering the hypothesis outlined above, and in order to investigate the γ-ray emission detected from 4C +55.17 in a framework that is more consistent with the observed properties of the source, we apply the dynamical model for the broad-band emission of CSOs proposed by Stawarz et al. (2008) and successfully tested against a sample of X-ray detected young radio galaxies of the CSO type by Ostorero et al. (2010). In this model, the newly born relativistic jets propagate across the inner region of the host galaxy and inject ultrarelativistic electrons into the compact lobes. These electrons, which provide the bulk of the internal lobes' pressure, cool radiatively and adiabatically within the sub-relativisticly expanding plasma, thus producing isotropic synchrotron (radio) and IC (X-ray to γ-ray) radiation. In the model, the broad-band emission spectra are evaluated self-consistently for a given set of the initial parameters of the central engine and of the host galaxy, taking into account the time-dependent evolution of the radiating electrons. For a given linear size of the system, which is uniquely related to a particular age of the system, the observed broad-band emission spectrum is given as a snapshot of the evolving multiwavelength radiation of the lobes. Based on this model, Stawarz et al. (2008) argued that, in fact, young radio galaxies should be detected by *Fermi*/LAT at GeV photon energies, albeit at low flux levels and after an exposure longer than one year. Other (physically distinct) scenarios for the production of soft, high energy, and VHE γ-rays in the lobes and hotspots of young radio galaxies have been proposed and investigated by Kino et al. (2007, 2009) and Kino & Asano (2010).

In the more detailed description of the model, the jets with total kinetic power ($L_{\rm j}$) propagate with the advance velocity ($v_{\rm h}$) in the interstellar medium, characterized by a given number density ($n_{\rm ext}$). At a particular instant of the source evolution, the inflated lobes will have a corresponding linear size (LS). The electrons injected through the termination shock into the lobes with the

intrinsically broken power-law energy distribution cool due to the synchrotron and IC processes. The most relevant ambient photon fields for the IC scattering are the UV emission of the accretion disk (mean photon energy $\varepsilon_{\rm disk} = 10\,{\rm eV}$, disk luminosity $L_{\rm disk}$), the starlight ($\varepsilon_{\rm star} = 0.83\,{\rm eV}$, host luminosity $L_{\rm star}$), and the infrared emission of the obscuring nuclear torus ($\varepsilon_{\rm dust} = 0.02\,{\rm eV}$, dust luminosity $L_{\rm dust}$). The magnetic field intensity is expressed in terms of the ratio of energy densities stored in the radiating electrons and the magnetic field, $U_{\rm e}/U_{\rm B}$, which is constant during the expansion of the radiating plasma. Note, however, that $U_{\rm e}$ and $U_{\rm B}$, as well as the energy densities of the ambient photon fields (and hence the electron cooling conditions) do change with time, and therefore depend on LS (see Stawarz et al. 2008, for more details).

The fit of the "young radio source" model to the collected broad-band dataset for 4C +55.17 is illustrated in Figure 3. In fitting the SED, we assume that the projected source size of the inner radio structure ($LS \simeq 400\,{\rm pc}$) is equal to the actual source size, though we note that this may be underestimated due to possible projection effects. Indeed, some amount of projection off the plane of the sky is required to account for the presence of the intense disk-related optical/UV continuum and the broad optical emission lines in the spectrum of 4C +55.17 (which might otherwise be completely obscured), as well as to account for the asymmetry in brightness between the two lobes. In fitting the broadband SED, the following model-free parameters were obtained: $L_{\rm j} \simeq 6.6 \times 10^{47}\,{\rm erg\,s^{-1}}$, $L_{\rm disk} \simeq 2 \times 10^{46}\,{\rm erg\,s^{-1}}$, $L_{\rm star} \simeq 10^{45}\,{\rm erg\,s^{-1}}$, $L_{\rm dust} \simeq 10^{45}\,{\rm erg\,s^{-1}}$, $U_{\rm e}/U_{\rm B} \simeq 160$, $v_{\rm h} \simeq 0.3c$, and $n_{\rm ext} \simeq 0.1\,{\rm cm^{-3}}$. The injection electron energy distribution is characterized by the minimum, break, and maximum electron Lorentz factors, $\gamma_{\rm min} \simeq 1$, $\gamma_{\rm br} \simeq 2 \times 10^4$, and $\gamma_{\rm max} \simeq 4 \times 10^5$, respectively, as well as by the low- and high-energy electron spectral indices, $s_1 \simeq 0.5$ and $s_2 \simeq 2.5$. The model fits quite successfully all the relevant data points within the low-frequency (radio) and high-frequency (hard X-ray to γ-ray IC component) ranges; it also reproduces nicely the spectral break within the *Fermi*/LAT photon energy range. We note that in our modeling here and below we do not consider γ-ray absorption effects related to the direct or reprocessed emission of the accretion disk, which may lead to the attenuation of the lobes' (or jets') emission at photon energies $> 100\,{\rm GeV}$ (see in this context Tanaka et al. 2011).

Looking closely at the UV part of the spectrum, we note an approximate factor of two difference between what is observed and what is required for producing the appropriate luminosity in IC-scattered γ rays. This can be resolved by recalling that in the framework of the model the optical/UV photon energy range is dominated by the thermal UV disk emission that may suffer from some non-neglible obscuration by the circumnuclear dust for moderate inclinations of the source to the line of sight. Also worth noting are the variation timescales of the disk, which are governed by the viscous motion within tens of gravitational radii from the black hole (Collier & Peterson 2001). This can account for the $\sim 30\%$ variation over seven years seen between the optical measurements from UVOT and SDSS (see § 2.2). On the other hand, the CSO-related non-thermal IC emission is expected to be non-variable in accordance with the observations, because this emission is produced within the hundred-pc-scale and sub-relativistictically expanding lobes, and hence the UV photons seen by the lobes' electrons will be averaged over the entire spatial extent of the radio structure.

Here we do not model the accretion-related emission in detail, but only roughly represent it as a blackbody component for the purpose of the evaluation of the IC radiation of the lobes. Likewise, the steep-spectrum soft X-ray continuum is not accounted for by the IC emission of compact lobes and instead may be attributed to the radiative output of the accretion disk and its corona (see Siemiginowska et al. 2008; Siemiginowska 2009, for the X-ray properties of young radio sources). Yet it should be also noted that the particular CSO model presented here cannot account for the millimeter–to–near infrared emission of 4C +55.17. In the framework of the discussed scenario, this has to be attributed to the radiation of the underlying jet, and not of the compact lobes.

The physical parameters of 4C +55.17 emerging from the model fit presented above may be compared with the physical parameters of bona fide young radio galaxies derived in the framework of the same model by Ostorero et al. (2010). The most significant differences can be noted in the kinetic luminosity of the jet ($L_{\rm j}$), the UV luminosity of the accretion disk ($L_{\rm disk}$), and the electron–to–magnetic field energy density ratio ($U_{\rm e}/U_{\rm B}$). In particular, the jet and the disk luminosities of 4C +55.17 are higher (by one to two orders of magnitude, on average) than the analogous luminosities of GPS radio galaxies. This is in fact expected, since the analyzed source is much more powerful than the relatively low-power radio galaxies modeled by Ostorero et al. (2010). The disk luminosity obtained from the fit can also be compared with the expected value based on the total luminosity of emission in broad lines ($L_{\rm BLR}$). Using eq. (1) in Celotti et al. (1997), along with the line fluxes of 4C +55.17 obtained in Wills et al. (1995) and the line ratios from Francis et al. (1991), we estimate the value of $L_{\rm BLR}$ to be $1.2 \times 10^{45}\,{\rm erg\,s^{-1}}$. Using the approximation $L_{\rm disk} \simeq 10 \times L_{\rm BLR}$, we thus obtain $L_{\rm disk} \simeq 1.2 \times 10^{46}\,{\rm erg\,s^{-1}}$, which again falls within a factor of two of the value obtained through the model, consistent with the level of uncertainty expected using this method.

3.1.2. Blazar Modeling

As already noted in the introduction, the lack of pronounced variability and resolved VLBI structure in 4C +55.17 would make it a highly unusual case of a blazar/FSRQ. Still, it is a worthwhile exercise to consider the physical parameters implied from the blazar model. In the framework of the blazar scenario the observed non-thermal emission of this source, including the γ-ray flux detected by *Fermi*/LAT, is expected to originate in the innermost parts of a relativistic jet that is closely aligned with the line of sight (e.g., Sikora et al. 1994). In this case, the broad-band emission of 4C +55.17 should be strongly Doppler boosted in the observer rest frame, and variable on short (days to weeks) timescales. The expected size of the blazar emission region (sub-pc), which is orders of magnitude smaller than the linear size of the resolved inner radio structure discussed previously ($\sim 400\,{\rm pc}$), as well as the presence of relativistic beaming effects, constitute the main differences between the "blazar" and "young radio source" scenarios.

In order to model the broad-band spectrum of 4C +55.17 as a blazar emission, we apply the dynamical model BLAZAR developed by Moderski et al. (2003) and later updated by Moderski et al. (2005) for the correct treatment of the Klein-Nishina regime (for applications of the model, see e.g.

Sikora et al. 2008; Kataoka et al. 2008). The model describes the production of the non-thermal emission by ultrarelativistic electrons, which are accelerated in situ within thin shells of plasma propagating along a conical relativistic jet (bulk Lorentz factor, $\Gamma_{\rm j} \gg 1$, jet opening angle $\theta_{\rm j} \sim 1/\Gamma_{\rm j}$) and which carry a fraction $L_{\rm e}/L_{\rm j}$ of the jet kinetic power. The acceleration process is attributed to the Fermi mechanism operating at strong shocks that are formed within the outflow as a result of the shells' collisions, which take place at distances greater than r_0 from the jet base, resulting in the injection of a broken power-law electron energy distribution into an emission region of linear size R and magnetic field intensity B. The non-thermal emission evaluated at $r \simeq R/\theta_{\rm j} \gtrsim r_0$ includes the synchrotron and IC components, with the target photons for the inverse-Compton scattering provided by the jet synchrotron radiation and the external photon fields (predominantly accretion disk emission reprocessed in the broad line region and within the dusty torus).

The BLAZAR fit to the broad-band spectrum of 4C +55.17 is shown in Figure 4. The fit was obtained with the following free parameters of the model: $L_{\rm j} \geq L_{\rm e} \simeq 6 \times 10^{42}\,{\rm erg\,s^{-1}}$, $L_{\rm disk} \simeq 3 \times 10^{46}\,{\rm erg\,s^{-1}}$, $L_{\rm dust} \simeq 6 \times 10^{45}\,{\rm erg\,s^{-1}}$, $r_0 \simeq 4 \times 10^{18}\,{\rm cm}$, $r \simeq 8 \times 10^{18}\,{\rm cm}$, $\Gamma_{\rm j} \simeq 12$, and $B \simeq 0.2\,{\rm G}$. For the injection electron energy distribution, the electron Lorentz factors $\gamma_{\rm min} \simeq 1$, $\gamma_{\rm br} \simeq 1.5 \times 10^3$, and $\gamma_{\rm max} \simeq 10^6$ were obtained, along with the spectral indices, $s_1 \simeq 0.5$ and $s_2 \simeq 2.8$. The blazar model fit to the collected dataset, and the implied physical parameters of the 4C +55.17 jet and its central engine, should be regarded as plausible. Notable differences with respect to the CSO model discussed previously can be however noted within the radio–to–X-ray frequency range. In particular, unlike the CSO fit, the blazar model fit does not account for the bulk of the observed radio fluxes. These emissions, in the framework of the blazar scenario, must therefore be produced further down the jet, at relatively large distances from the blazar emission zone. On the other hand, the high-energy tail of the synchrotron blazar emission dominates the radiative output of the system around the observed near-infrared and optical frequencies, and also at soft X-rays. The observed hard X-ray spectrum of 4C +55.17 can be hardly attributed to the IC blazar emission and requires an additional spectral component. In general, the CSO and blazar fits differ the most within the near infrared and X-ray domains, hence future constraints on the hard X-ray and near infrared spectra, along with continued monitoring from the radio to the γ-ray band, should be considered as a potential way of discriminating between the two scenarios.

In comparing these two models, we also note the important difference between the blazar and CSO model for 4C +55.17 in the radiative efficiency of the emission zone. Compact emission zones of blazar sources are typically characterized by a very low (less than a few percent) radiative efficiency (e.g., Sikora et al. 1994). In this context, only a small fraction of the jet kinetic power is dissipated in the blazar emission zone and radiated away in the form of high-energy emission, which is strongly Doppler-boosted in the observer frame due to the relativistic bulk velocity of the emitting plasma. This is also the case for 4C +55.17 when modeled in the framework of the blazar scenario discussed above. On the other hand, the radiative efficiency of the sub-relativistically expanding lobes of young radio sources is known to be large, often exceeding 10% (De Young 1993; Stawarz et al. 2008), which naturally accounts for the particularly high intrinsic radio luminosity of

these sources, being comparable to the most powerful radio galaxies and quasars (Readhead et al. 1996). Likewise, when modeling 4C +55.17 as a CSO, the radiative efficiency was similarly high. The improved radiative efficiency of CSO sources, together with the relatively high jet kinetic power implied by the young radio source scenario (higher than that implied by the blazar model), can thus account for the observed γ-ray luminosity even in the absence of relativistic beaming.

While the CSO-type and blazar modelings of the broad-band spectrum of 4C +55.17 can both account for the γ-ray emission from the source, we find the implied value for the bulk Lorentz factor $\Gamma_{\rm j} \simeq 12$ under the blazar scenario difficult to reconcile with its observed VLBI properties. The physical mechanism responsible for the steady γ-ray emission is also not easily explained under this framework. Still, the unusual characteristics of 4C +55.17 as for a young radio source may be evidence for a combination of radiation produced in the sub-pc scale relativistic jet and the emission of the compact lobes. The modeling of this complex scenario, which might require a combination of the two models discussed above, is beyond the scope of the present work. A similar situation was recently considered by Migliori (in prep), who have studied the high-energy (X-ray to γ-ray) emission of radio-loud quasars with CSO-type inner radio morphology, such as, e.g., 3C 186. Objects of that type might be very common in scenarios of intermittent jet production in active galaxies, proposed to account for the evolution of radio-loud AGNs (e.g., Reynolds & Begelman 1997; Siemiginowska et al. 2007; Czerny et al. 2009, and references therein). With its complex radio structure featuring inner and outer lobes, as well as jet-like features (Rossetti et al. 2005; Tavecchio et al. 2007), 4C +55.17 might thus be another example of AGN with intermittent jet production.

3.2. High Energy γ-ray Continuum of 4C +55.17

At energies $\gtrsim 10\,\mathrm{GeV}$ the γ-ray continua of high-redshift sources begin to suffer from substantial attenuation by the still poorly known EBL photon field due to the photon-photon pair creation process (Hauser & Dwek 2001). By attributing the attenuation of AGN γ-ray spectra to these interactions, it is thus possible to place significant upper limits to the EBL provided some estimate of the source's intrinsic spectrum (Aharonian et al. 2006). In this respect, combined *Fermi* and VHE measurements by Cherenkov telescopes such as MAGIC, H.E.S.S., and VERITAS, continue to prove successful at providing these limits (e.g. Georganopoulos et al. 2010; Aleksić at al. 2011; Orr et al. 2011). Furthermore, with the VHE detection of the FSRQ 3C 279 ($z = 0.536$) by MAGIC (Albert et al. 2008), and the recently announced detections of others quasars – PKS 1510–089 ($z = 0.361$) by H.E.S.S. (Wagner & Behera 2010) and PKS 1222+216 ($z = 0.432$) by MAGIC (Aleksić at al. 2011) – the search for increasingly distant luminous sources in the observable range of ground-based Cherenkov Telescopes has become one of considerable interest to the TeV community.

The extension of the observed γ-ray spectrum of 4C +55.17 up to energies of 145 GeV, coupled with the source's relatively high redshift of $z = 0.896$, immediately places it among the most important high-z objects that can be used for constraining the widely debated EBL level even within

LAT energies; for an overview of different methods for constraining the EBL with the *Fermi*/LAT, see Abdo et al. (2010c). Figure 5 illustrates the $\tau_{\gamma\gamma}$ opacity at the redshift $z = 0.896$ due to γ-ray absorption with the EBL intensity and spectral distribution for various models (Finke et al. 2010; Franceschini et al. 2008; Gilmore et al. 2009; Kneiske et al. 2004; Stecker et al. 2006) considered as a function of photon energy. The highest-energy photon associated with 4C +55.17 is also indicated. As illustrated in the figure, attenuation due to the EBL-related absorption of γ-rays within the observed range is predicted in all the scenarios, including those close to the lower limits derived from galaxy counts (e.g., Franceschini et al. 2008; Finke et al. 2010; Gilmore et al. 2009).

To test the validity of particular models of the EBL using the 4C +55.17 spectrum, we followed the likelihood ratio test method described in Abdo et al. (2010c). The full > 100 MeV observed spectrum was first fit to a broken power law with EBL attenuation from 9 separate EBL models (Finke et al. 2010; Franceschini et al. 2008; Gilmore et al. 2009; Primack et al. 2005; Stecker et al. 2006; Salamon & Stecker 1998; Kneiske et al. 2004), with the normalization of the attenuation parameter $\tau_{\gamma\gamma}(E, z = 0.896)$ fixed to 1 at all energies. The results from each of the spectral fits, including the low (Γ_1) and high (Γ_2) broken power law indices, as well as the integral flux values, are summarized in Table 2. Allowing the normalization of the predicted opacity $\tau_{\gamma\gamma}$ to remain free, we then compared each result with the likelihood values obtained when the normalization parameter was fixed to 1. In cases where the $\tau_{\gamma\gamma}$ normalization was reduced, a rejection at the level of n standard deviations (σ) of the particular model could be established using the formula:

$$n = \sqrt{-2 \times [\log(L_{\rm fixed}) - \log(L_{\rm free})]}\,, \tag{1}$$

where $L_{\rm fixed}$ and $L_{\rm free}$ are the likelihood values of the fits for fixed and free normalizations on $\tau_{\gamma\gamma}$, respectively. Using these results, we were able to reject two separate models at $> 3\sigma$ significance. These were the Stecker et al. (2006) baseline and fast evolution models at 3.9σ and 4.3σ, respectively, with preferred normalizations of 0.17 ± 0.14 and 0.16 ± 0.12. These models were similarly rejected in Abdo et al. (2010c) by applying the likelihood ratio test to several blazars and gamma-ray bursts with redshifts ranging from $z = 1.05$ to $z = 4.24$. Combining this result with the overall rejection significance of the Stecker et al. (2006) baseline model of 11.4σ as calculated in Abdo et al. (2010c, § 3.2.3 therein), we obtain a new combined rejection of 11.7σ for both the baseline and fast evolution models.

Figure 6 shows the predicted shape of the intrinsic spectrum of 4C +55.17 obtained by deabsorbing the observed *Fermi* spectrum using the Stecker et al. (2006) baseline EBL model. A common feature occurring from models which over-predict the level of EBL is that of an unbounded exponential spectral rise at highest energies – a behavior which can largely be considered nonphysical, and has thus been used in previous studies to place constraints on the EBL using TeV observations (e.g., Dwek & Krennrich 2005). This behavior is clearly illustrated in the case of the Stecker et al. (2006) baseline model. Such a feature would in turn require the modeling of an additional spectral component beyond that which we consider in § 3.1 and that would be orders of

magnitude more luminous than the observed inverse-Compton (IC) peak. We also note that any intrinsic *absorption* that may be taking place within the source represents an even greater rejection of this model, as the true attenuation due to the EBL would be even less. We therefore consider the Stecker et al. (2006) baseline and fast evolution[27] models to over-predict the true level of EBL at the observed redshift and energies.

With its excellent sensitivity in the high-energy range, the LAT instrument provides a unique opportunity to search for VHE candidates at high redshifts through detailed spectral analysis of the *Fermi* data. In the case of 4C +55.17, the attenuated high-energy spectrum obtained from fitting the nine often discussed EBL models is illustrated in Figure 7. Each spectrum is extrapolated beyond the highest observed photon energy of 145 GeV and compared against the typical differential flux sensitivity curves of currently operating TeV telescopes. With the exception of the four "highest-level" EBL models (including the two models ruled out by the present work), the observed 4C +55.17 spectrum is found to lie at the observable threshold for ground-based observations. It is also worth noting that while intrinsic absorption from interactions with the UV disk and infrared torus may contribute to the spectral attenuation at energies > 100 GeV, this effect would be reduced in cases where the γ-ray emission takes place at hundreds-of-parsecs scale distances from the central black hole, for which there is compelling evidence in the case of 4C +55.17 (see § 3.1.1). In addition, with the present analysis we find no evidence of variability in 4C +55.17 over 19 months of LAT observing time, and furthermore we find its flux to be consistent with the EGRET measured value, thus showing no evidence of variability at γ-ray energies over decade timescales as well. The non-variable γ-ray continuum of the source thus promises the opportunity to observe it over the extended timescales required for a 5σ detection. This is in contrast to the other VHE-detected quasars, which were detected only during periods where the sources were in a flaring state. In this way 4C +55.17 stands apart from all of the EBL-constraining sources considered in Abdo et al. (2010c), as it holds the greatest potential for providing future constraints.

4. Conclusions

The investigation of the multiwavelength properties of 4C +55.17, including its unusually hard γ-ray spectrum, lack of distinct variability, and CSO-like radio morphology, has highlighted the exceptional nature of this γ-ray source. For the first time, we have modeled the radio to γ-ray emission of 4C +55.17 as a young radio source using a dynamic model that is consistent with the full extent of its observed properties. Furthermore, we find that the prospect of a VHE observation of 4C +55.17, whose γ-ray spectrum already extends up to the observed energy of 145 GeV, is within reach of the current generation of Cherenkov telescopes. A detection by such an instrument would not only add to the present understanding of the source itself, but would also serve to place

[27]Because the Stecker et al. (2006) fast evolution model predicts an increased opacity from the baseline model, our conclusions from the baseline test can be applied in both cases.

a significant upper limit to the level of EBL through combined *Fermi* and VHE data. Furthermore, we anticipate that through continued monitoring of 4C +55.17 at high energies with the *Fermi* LAT, as well as in the radio through X-rays, the precise classification of 4C +55.17 will become increasingly more apparent. If, for example, the source continues to remain non-variable in γ-rays in the years to come, its average flux versus variability may eventually lie outside the distribution of *Fermi* γ-ray emitting blazars altogether, which would make any standard blazar emission scenario difficult to reconcile. On the other hand, if rapid variability is found in this source, that would seem to rule out a pure CSO interpretation. Thus we expect that 4C +55.17 will be an important target for future observations across all wavelengths.

The *Fermi* LAT Collaboration acknowledges generous ongoing support from a number of agencies and institutes that have supported both the development and the operation of the LAT as well as scientific data analysis. These include the National Aeronautics and Space Administration and the Department of Energy in the United States, the Commissariat à l'Energie Atomique and the Centre National de la Recherche Scientifique / Institut National de Physique Nucléaire et de Physique des Particules in France, the Agenzia Spaziale Italiana and the Istituto Nazionale di Fisica Nucleare in Italy, the Ministry of Education, Culture, Sports, Science and Technology (MEXT), High Energy Accelerator Research Organization (KEK) and Japan Aerospace Exploration Agency (JAXA) in Japan, and the K. A. Wallenberg Foundation, the Swedish Research Council and the Swedish National Space Board in Sweden.

Additional support for science analysis during the operations phase is gratefully acknowledged from the Istituto Nazionale di Astrofisica in Italy and the Centre National d'Études Spatiales in France.

L.O. acknowledges support by a 2009 National Fellowship "L'ORÉAL Italia Per le Donne e la Scienza" of the L'ORÉAL-UNESCO program "For Women in Science," and partial support from the INFN grant PD51 and the ASI Contract No. I/016/07/0 COFIS. Ł.S. is grateful for the support from Polish MNiSW through the grant N-N203-380336. R.M. was supported by the MNiSW grant no. N-N203-301635

The authors acknowledge the support by the *Swift* team for providing ToO observations and the use of the public HEASARC software packages.

The authors would like to thank Annalisa Celotti, Luigi Costamante, Berrie Giebels, and Dave Thompson for their helpful comments and suggestions.

A. Association of the 145 GeV photon with 4C +55.17

To further investigate the VHE detection of the source, the 145 GeV event was analyzed in detail using the event display[28] and found to be a clean γ-ray event, going through more than half a tracker tower before interacting in the back planes and generating a well-behaved symmetric shower in the calorimeter. A full Monte Carlo simulation was also run in order to determine the accuracy of the energy reconstruction. A total of $500,000$ γ-rays between the energies 50 and 200 GeV were simulated at an incoming angle θ and ϕ equivalent to that of the measured event. Data selection cuts were applied on all similar variables, including cuts on the calorimeter raw energy, best measured energy, reconstructed direction, and event class level. The distribution in Monte Carlo energy for the remaining events was found to give a $\sim 1\sigma$ error of ± 11 GeV.

The probability of the 145 GeV event occurring by random coincidence from background contamination was calculated using the `gtsrcprob` analysis tool. Probabilities of each event are assigned via standard likelihood analysis to all sources within a provided best-fit model (Mattox et al. 1996). The probability that a photon is produced by a source i is proportional to $M_{\rm i}$, given by the formula:

$$M_{\rm i}(\varepsilon', \hat{p}', t) = \int_{\rm SR} d\varepsilon \, d\hat{p} \; S_{\rm i}(\varepsilon, \hat{p}) \; R(\varepsilon', \hat{p}'; \varepsilon, \hat{p}, t) \, , \tag{A1}$$

where $S_{\rm i}(\varepsilon, \hat{p})$ is the predicted counts density from the source at energy ε and position $\hat{p}$, and $R(\varepsilon', \hat{p}'; \varepsilon, \hat{p}, t)$ is the convolution over the instrument response. In this way, all the surrounding point sources, the diffuse background, and their corresponding best-fit spectra are taken into account when assigning probabilities to individual photon events. For the 145 GeV event, the probability of spurious association with 4C +55.17 was found to be 1.8×10^{-3}, agreeing well with an independent method by Neronov et al. (2010), who quote a chance probability by background contamination of 3.1×10^{-3} for the same event.

B. Calculation of the MAGIC II and VERITAS Differential Flux Sensitivities

Starting with the integral flux sensitivity curves of MAGIC II (Borla Tridon et al. 2010) and VERITAS (Perkins & Maier 2009), the differential flux sensitivities can be derived for a given functional form. In the case of 4C +55.17, we may represent the attenuated VHE spectrum in general with an exponential cutoff given by the formula:

$$\frac{dN}{dE} = N_0 \, E^{-\Gamma} \, e^{-(\frac{E}{E_{\rm c}})} \tag{B1}$$

[28] `http://glast-ground.slac.stanford.edu/DataPortalWired/`

where N_0, E_c, and Γ are free parameters of the fitted form of the function. The integral flux above some minimum energy E_o is thus given by:

$$N = N_0 \int_{E_0}^{\infty} dE\ E^{-\Gamma}\ e^{-\frac{E}{E_c}} \tag{B2}$$

Defining the quantity

$$\Psi(E) \equiv \int_{E_0}^{\infty} dE\ E^{-\Gamma}\ e^{-\frac{E}{E_c}} \tag{B3}$$

the appropriate solution for N_0 may be substituted into equation B1 to obtain:

$$\left.\frac{dN}{dE}\right|_{E_0} = \frac{N\,E_0^{-\Gamma}\,e^{-(\frac{E_0}{E_c})}}{\Psi(E_0)} \tag{B4}$$

To construct the differential flux sensitivity curves, we obtained the values $\Gamma = 2.12$ and $E_c = 100$ GeV by performing a `gtlike` fit of the > 1.6 GeV data of 4C +55.17 to the exponential cutoff functional form. For each value N of the integral flux sensitivity, a corresponding differential flux sensitivity value could thus be obtained via numerical evaluation of equation B4.

REFERENCES

Abdo, A., et al. (Fermi-LAT collaboration), 2009a, ApJS, 183, 46

Abdo, A., et al. (Fermi-LAT collaboration), 2009b, ApJ, 700, 597

Abdo, A., et al. (Fermi-LAT collaboration), 2010a, ApJ, 188, 405

Abdo, A., et al. (Fermi-LAT collaboration), 2010b, ApJ, 715, 429

Abdo, A., et al. (Fermi-LAT collaboration), 2010c, ApJ, 723, 1082

Adelman-McCarthy, J. K., et al. 2008, ApJS, 175, 297

Aharonian, F., et al. 2006, Nature, 440, 1018

Ajello, M., et al. 2008, ApJ, 673, 96

Ajello, M., et al. 2009, ApJ, 699, 603

Albert, J., et al. (MAGIC collaboration), 2008, Science, 320, 1752

Aleksić, J. et al. 2011, ApJ, 730, L8

608 Altschuler, D. R., & Wardle, J. F. C. 1976, MmRAS, 82, 1

609 Atwood, W. B., et al. (Fermi-LAT collaboration) 2009, ApJ, 697, 1071

610 Augusto, P., Gonzalez-Serrano, J. I., Perez-Fournon, I., & Wilkinson, P. N. 2006, MNRAS, 368,
611 1411

612 Baum, S. A., O'Dea, C. P., Murphy, D. W., & de Bruyn, A. G. 1990, A&A, 232, 19

613 Begelman, M. C. 1996, in Cygnus A: Study of a Radio Galaxy, eds. C. L. Carilli & D. E. Harris
614 (Cambridge: Cambridge Univ. Press), 209

615 Begelman, M. C. 1999, in The Most Distant Radio Galaxies, eds. H. J. A. Röttgering, P. N. Best,
616 & M. D. Lehnert, 173

617 Bicknell, G. V., Dopita, M. A., & O'Dea, C. P. O. 1997, ApJ, 485, 112

618 Bloom, S. D., Marscher, A. P., Gear, W. K., Terasranta, H., Valtaoja, E., Aller, H. D., & Aller,
619 M. F. 1994, AJ, 108, 398B

620 Borla Tridon, D., Schweizer, T., Goebel, F., Mirzoyan, R., & Teshima, M. 2010, Nucl. Instrum.
621 Methods Phys. Res., A623, 437

622 Burn, B. J. 1966, MNRAS, 133, 67

623 Burrows, D. N., et al. 2005, Space Science Reviews, 120, 165

624 Cardelli, J. A., Clayton, G. C., & Mathis, J. S. 1989, ApJ, 345, 245

625 Carvalho, J. C. 1994, A&A, 292, 392

626 Carvalho, J, C. 1998, A&A, 329, 845

627 Casandjian, J.-M., & Grenier, I. A. 2008, A&A, 489, 849

628 Celotti, A., Padovani, P., & Ghisellini, G. 1997, MNRAS, 286, 415

629 Cohen, M., Wheaton, Wm. A., & Megeath, S. T. 2003, AJ, 126, 1090

630 Collier, S., & Peterson, B. M. 2001, ApJ, 555, 775

631 Comastri, A., Fossati, G., Ghisellini, G., & Molendi, S. 1997, ApJ, 480, 534

632 Cutri, R. M., et al. 2003, The IRSA 2MASS All-Sky Point Source Catalog, NASA/IPAC Infrared
633 Science Archive. `http://irsa.ipac.caltech.edu/applications/Gator/`

634 Czerny, B., Siemiginowska, A., Janiuk, A., Nikiel-Wroczyński, B., & Stawarz, Ł. 2009, ApJ, 698,
635 840

de Vries, W. H., Barthel, P. D., & O'Dea, C. P. 1997, A&A, 321, 105

De Young, D. S. 1993, ApJ, 402, 95

De Young, D. S. 1997, ApJ, 490, L55

Dwek, E., & Krennrich, F., 2005 ApJ, 618, 657

Fanti, R., et al. 1990, A&A, 231, 333

Fanti, C., Fanti, R., Dallacasa, D., Schillizi, R. T., Spencer, R. E., Stanghellini, C. 1995, A&A, 302, 317

Fey, A. L., et al. 2004, AJ, 127, 3587

Finke, J. D., Razzaque, S., & Dermer, C. D. 2010, ApJ, 712, 238

Franceschini, A., Rodighiero, G., & Vaccari, M. 2008, A&A, 487, 837

Francis, P. J., Hewett, P. C., Foltz, C. B., Chaffee, F. H., Weymann, R. J., & Morris, S. L. 1991, ApJ, 373, 465

Garcia-Burillo, S., Combes, F., Neri, R., Fuente, A., Usero, A., Leon, S., & Lim, J. 2007, A&A, 468, L71

Gehrels, N., et al. 2004, ApJ, 611, 1005

Georganopoulos, M., Finke, J., & Reyes, L. 2010, ApJ, 714, L157

Gilmore, R. C., Madau, P., Primack, J. R., Somerville, R. S., & Haardt, F. 2009, MNRAS, 399, 1694

Gugliucci, N. E., Taylor, G. B., Peck, A. B., & Giroletti, M. 2007, ApJ, 661, 78

Hartman, R. C., et al. 1999, ApJS, 123, 79

Hauser, M. G., & Dwek, E. 2001, ARA&A, 39, 249

Helmboldt, J. F., et al. 2007, ApJ, 658, 203

Huang, L., Jiang, D., & Cao, X. 1998, Chinese Physics Letters, 15, 856

Jackson, N., Battye, R. A., Browne, I. W. A., Joshi, S., Muxlow, T. W. B., & Wilkinson, P. N. 2007, MNRAS, 376, 371

Jenness, T., Robson, E. I., & Stevens, J. A. 2010, MNRAS, 401, 1240

Kataoka, J., et al. 2008, ApJ, 672, 787

Kawakatu, N., & Kino, M. 2006, MNRAS, 370, 1513

664 Kino, M., Kawakatu, N., & Ito, H. 2007, MNRAS, 376, 1630

665 Kino, M., Ito, H., Kawakatu, N., & Nagai, H. 2009, MNRAS, 395, L43

666 Kino, M., & Asano, K. 2011, MNRAS, in press

667 Kneiske, T. M., Bretz, T., Mannheim, K., & Hartmann, D. H. 2004, A&A, 413, 807

668 Kovalev, Y. Y., et al. 2009, ApJ, 696, 17

669 Luo, W.-F., Yang, J., Cui, L., Liu, X., & Shen, Z.-Q. 2007, ChJAA, 7, 611

670 Marscher, A. P., Jorstad, S. G., Mattox, J. R., & Wehrle, A. E. 2002, ApJ, 577, 85

671 Mattox, J. R., et al. 1996, ApJ, 461, 396

672 Mattox, J. R., Hartman, R. C., & Reimer, O. 2001, ApJS, 135, 155

673 Moderski, R., Sikora, M., & Błażejowski, M. 2003, A&A, 406, 855

674 Moderski, R., Sikora, M., Coppi, P. S., & Aharonian, F. 2005, MNRAS, 363, 954

675 Myers, S. T., et al. 2003, MNRAS, 341, 1

676 Neronov, A., Semikoz, D., & Vovk, Ie. 2010 A&A, 529, 59

677 O'Dea, C. P. 1998, PASP, 110, 493

678 O'Dea, C. P., & Baum, S. A. 1997, AJ, 113, 148

679 Ostorero, L., et al. 2010, ApJ, 715, 1071

680 Orienti, M., & Dallacasa, D. 2008, A&A, 487, 885

681 Orr, M. R., Krennrich, F., & Dwek, E., submitted (arXiv:1101.3498)

682 Peck, A. B., Taylor, G. B., & Conway, J. E. 1999, ApJ, 521, 103

683 Perkins, J. S., & Maier, G. 2009, in eConf Proceedings of the 2009 Fermi Symposium, C091122

684 Perucho, M., & Marti, J. M. 2002, ApJ, 568, 639

685 Philips, R. B., & Mutel, R. L. 1982, A&A, 405, 499

686 Primack, J. R., Bullock, J. S., Somerville, R. S. (2005) AIPC, 745, 23

687 Readhead, A. C. S., Taylor, G. B., Xu, W., Pearson, T. J., Wilkinson, P. N., & Polatidis, A. G.
688 1996, ApJ, 460, 612

689 Reid, A., Shone, D. L., Akujor, C. E., Browne, I. W. A., Murphy, D. W., Pedelty, J., Rudnick, L.,
690 & Walsh, D. 1995, A&AS, 110, 213

691 Reich, W., Reich, P., Pohl, M., Kothes, R., & Schlickeiser, R. 1998, A&AS, 131, 11

692 Reynolds, C. S., & Begelman, M. C. 1997, ApJ, 487, L135

693 Rieke, G. H., & Lebofsky, M. J. 1985, ApJ, 288, 618

694 Roming, P. W. A., et al. 2005, Space Science Reviews, 120, 95

695 Rossetti, A., Mantovani, F., Dallacasa, D., Fanti, C., & Fanti, R. 2005, A&A, 434, 449

696 Salamon, M. H., & Stecker, F. W. 1998, ApJ, 493, 547

697 Schlegel, D. J., Finkbeiner, Davis, M. 1998, ApJ, 500, 525

698 Schneider, D. P., et al. 2007, AJ, 134, 102

699 Seielstad, G. A., Pearson, T. J., & Readhead, A. C. S. 1983, PASP, 95, 842

700 Siemiginowska, A., Cheung, C. C., LaMassa, S., Burke, D. J., Aldcroft, T. L., Bechtold, J., Elvis,
701 M., & Worrall, D. M. 2005, ApJ, 632, 110

702 Siemiginowska, A., Stawarz, Ł., Cheung, C. C., Harris, D. E., Sikora, M., Aldcroft, T. L., &
703 Bechtold, J. 2007, ApJ, 657, 145

704 Siemiginowska, A., LaMassa, S., Aldcroft, T. L., Bechtold, J., & Elvis, M. 2008, ApJ, 684, 811

705 Siemiginowska, A. 2009, Astron. Nach., 330, 264

706 Sikora, M., Begelman, M. C., & Rees, M. J. 1994, ApJ, 421, 153

707 Sikora, M., Moderski, R., & Madejski, G. M. 2008, ApJ, 675, 71

708 Snellen, I. A. G., Schilizzi, R. T., Miley, G. K., de Bruyn, A. G., Bremer, M. N., & Röttgering,
709 H. J. A. 2000, MNRAS, 319, 445

710 Stawarz, Ł., Ostorero, L., Begelman, M. C., Moderski, R., Kataoka, J., & Wagner, S. 2008, ApJ,
711 680, 911

712 Stecker, F. W., Malkan, M. A., & Scully, S. T. 2006, ApJ, 648, 774

713 Tanaka, Y. T., et al. 2011, ApJ, in press (arXiv:1101.5339)

714 Tavecchio, F., Maraschi, L., Wolter, A., Cheung, C. C., Sambruna, R. M., & Urry, C. M. 2007,
715 ApJ, 662, 900

716 Taylor, G. B., et al. 2007, ApJ, 671, 1355

717 Teräsranta, H., et al. 1998, A&AS, 132, 350

718 Teräsranta, H., et al. 2004, A&A, 427, 769

719 Teräsranta, H., Wiren, S., Koivisto, P., Saarinen, V., & Hovatta, T. 2005, A&A, 440, 409

720 Torniainen, I., Tornikoski, M., Lähteenmäki, A., Aller, M. F., Aller, H. D., Mingaliev, M. G. 2007,
721 A&A, 469, 451

722 Urry, C. M., & Padovani, P. 1995, PASP, 107, 803

723 van Breugel, W., Miley, G., & Heckman, T. 1984, AJ, 89, 5

724 Veron-Cetty, M. P. & Veron, P., 2006, A&A, 455, 773

725 Wagner, S., & Behera, B. (H.E.S.S. collaboration) 2010, in 11th HEAD Meeting, BAAS, 41, 660

726 Wardle, J. F. C., Bridle, A. H., & Kesteven, M. J. L. 1981, AJ, 86, 848

727 Wilkinson, P. N., Polatidis, A. G., Readhead, A. C. S., Xu, W., & Pearson, T. J. 1994, ApJ, 432,
728 L87

729 Wills, B. J., et al. 1995, ApJ, 447, 139

730 Wright, E. L., et al. 2009, ApJS, 180, 283

Table 1. *Swift*/UVOT Observations of 4C +55.17

Band	λ [Å]	$F_{\rm ep1}$ [mJy]	$F_{\rm ep2}$ [mJy]	$F_{\rm ep3}$ [mJy]
V	5402	0.331 ± 0.061	0.337 ± 0.029	..
B	4329	0.262 ± 0.015	0.286 ± 0.015	..
U	3501	0.249 ± 0.010	0.251 ± 0.011	..
UVW1	2634	0.175 ± 0.007	0.174 ± 0.007	..
UVM2	2231	0.142 ± 0.029	0.167 ± 0.007	..
UVW2	2030	0.125 ± 0.009	0.127 ± 0.005	0.130 ± 0.005

Note. — The observations were obtained on 2009 March 5 (ep1), Nov 11 (ep2), and Nov 26 (ep3).

Table 2. De-absorption of γ-ray flux using different EBL models with fixed $\tau_{\gamma\gamma}$ normalization

EBL model	Γ_1	Γ_2	Flux[a]	-log(likelihood)
Finke et al. (2010)	1.83 ± 0.05	2.20 ± 0.06	9.05 ± 0.46	595671.252
Franceschini et al. (2008)	1.83 ± 0.05	2.21 ± 0.06	9.04 ± 0.46	595671.192
Gilmore et al. (2009)	1.83 ± 0.05	2.21 ± 0.06	9.04 ± 0.46	595671.133
Primack et al. (2005)	1.83 ± 0.05	2.19 ± 0.06	9.06 ± 0.46	595671.074
Kneiske (2004) best fit	1.83 ± 0.05	2.18 ± 0.06	9.06 ± 0.46	595671.577
Kneiske (2004) high UV	1.84 ± 0.05	2.14 ± 0.06	9.10 ± 0.46	595672.025
Stecker (2006) baseline	1.85 ± 0.05	2.10 ± 0.06	9.14 ± 0.46	595678.519
Stecker (2006) fast evolution	1.85 ± 0.05	2.10 ± 0.07	9.14 ± 0.46	595680.170
Salamon & Stecker (1998)	1.84 ± 0.05	2.15 ± 0.06	9.10 ± 0.46	595673.291

[a]Flux above 100 MeV in units of $[10^{-8}\,{\rm cm}^{-2}\,{\rm s}^{-1}]$

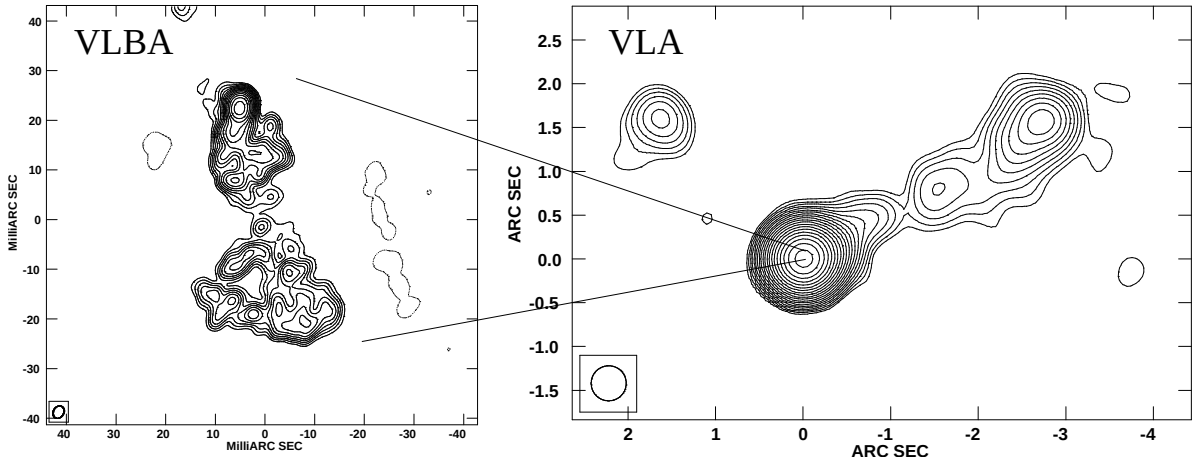

Fig. 1.— VLBA 5 GHz map (left) featuring the inner parsec-scale radio structure of 4C +55.17, reimaged using data from Helmboldt et al. (2007). The beam size is 2.0 mas × 1.6 mas (position angle = $-29.6°$), and the contour levels increase by factors of $\sqrt{2}$ beginning at 1 mJy/beam. The resolved morphology has a total angular size of 53 mas (413 pc). The VLA 5 GHz map (right) with a $0.4''$ beam (lowest contour is 2 mJy/beam increasing by factors of $\sqrt{2}$) shows the large scale radio structure (from Tavecchio et al. 2007).

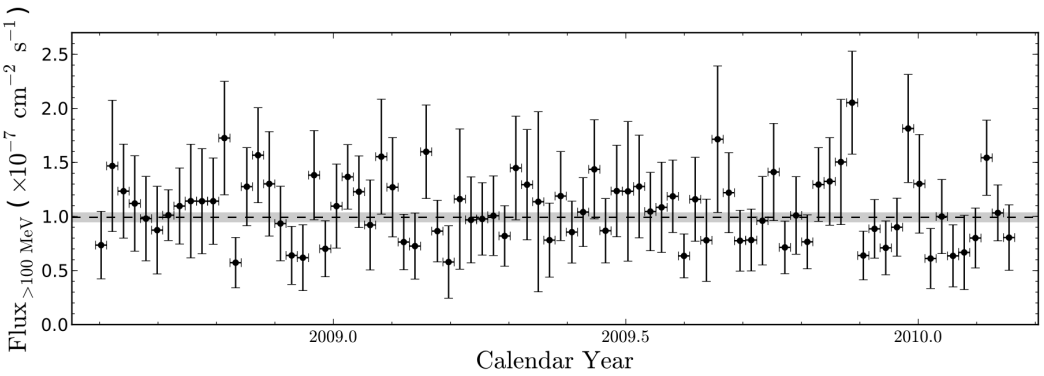

Fig. 2.— *Fermi*/LAT 19-month γ-ray light curve of 4C +55.17 divided into 7 day bins. All points represent $> 3\sigma$ detections and are plotted along with their statistical errors. The dashed horizontal line and gray region represent the weighted mean and corresponding error derived from all $> 3\sigma$ detections over the observing period.

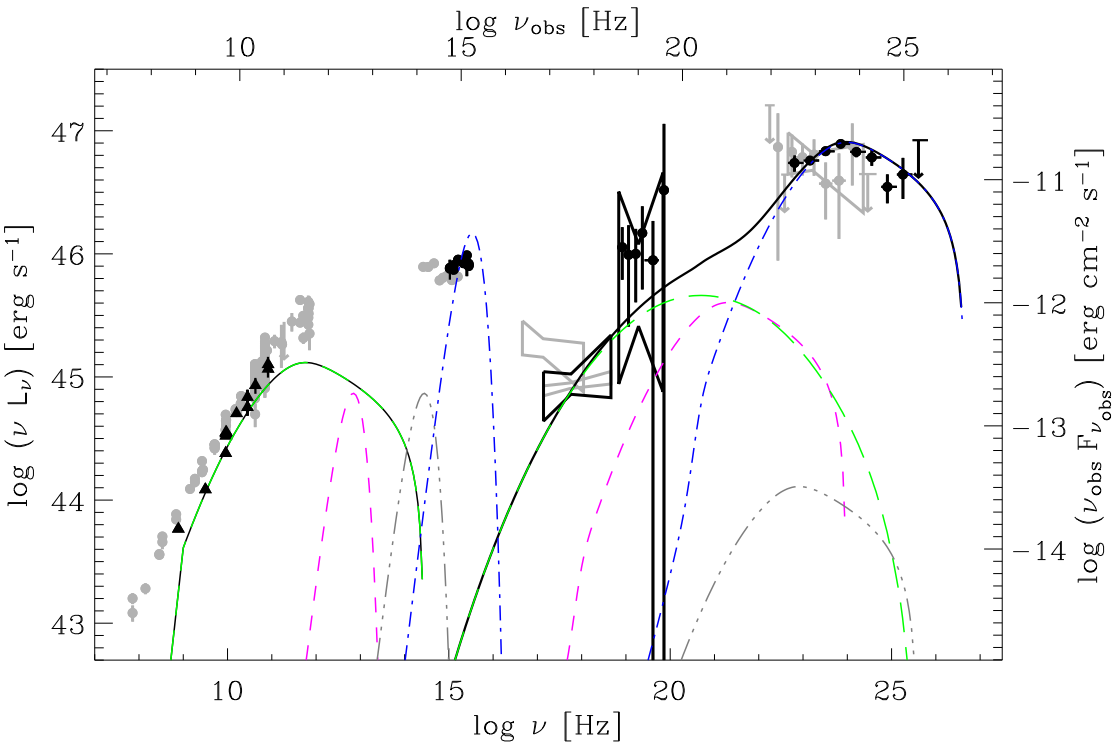

Fig. 3.— The CSO model of 4C +55.17 versus multiwavelength data, including the new LAT spectrum along with contemporaneous data with *Swift* XRT, BAT, and UVOT (black bullets). Archival detections (gray) with EGRET (Hartman et al. 1999), ROSAT, Chandra, SDSS, 2MASS, 5-year integrated WMAP, and historic radio data are also included, as well as archival VLA measurements (black triangles) of the inner $\sim$ 400pc radio structure (see § 2.2). De-absorption of the observed *Fermi* spectral points using the Finke et al. (2010) EBL model was applied in order to properly model the intrinsic γ-ray spectrum. Black curves indicate the total non-thermal emission of the lobes, with the long-dashed/green representing the contribution from synchrotron self-Compton (SSC). Dashed/pink, dash-dot-dotted/gray, and dash-dotted/blue blackbody-type peaks represent the dusty torus, starlight, and the UV disk emission components, respectively, along with their corresponding inverse-Compton components as required by the model.

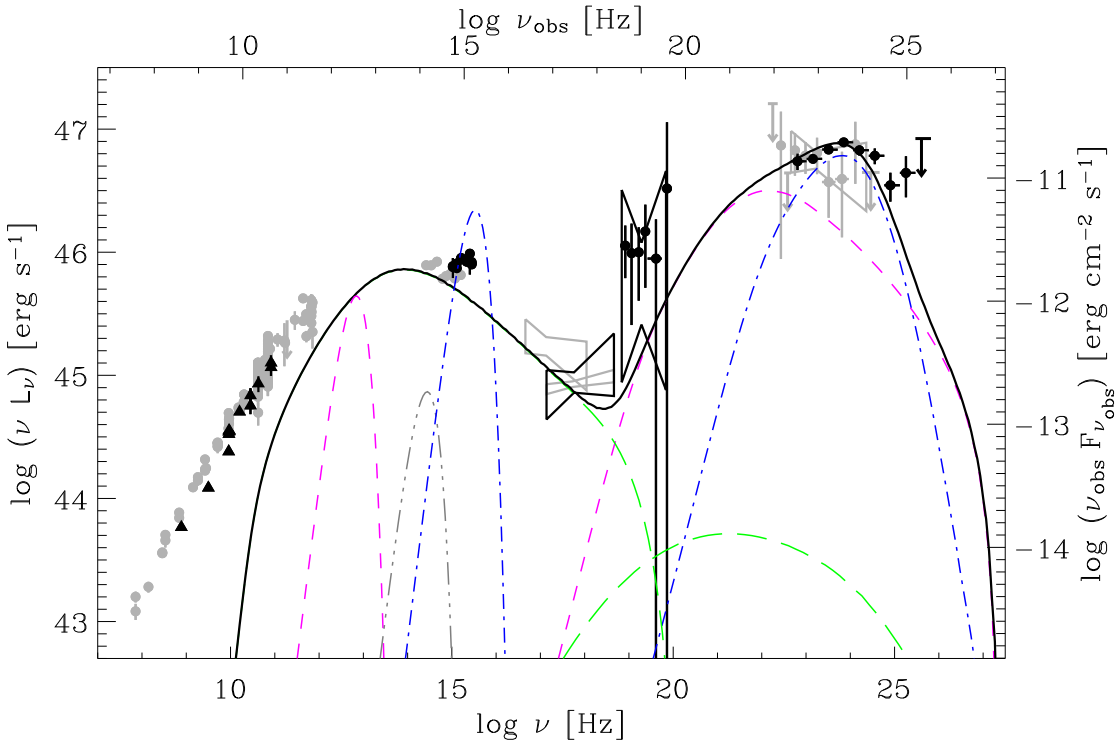

Fig. 4.— Blazar fit using multi-wavelength data for 4C +55.17. Indicated are the individual contributions from synchrotron and SSC (long-dashed/green), as well as IC scattering off of the reprocessed UV disk emission from the broad line region (dash-dotted/blue), dusty torus (dashed/pink), and host galaxy (dash-dot-dotted/gray); the black curve indicates the total of these components. As in Fig. 3, the dashed/pink, dash-dot-dotted/gray, and dash-dotted/blue blackbody-type peaks represent the dusty torus, starlight, and the UV disk emission components, respectively, along with their corresponding inverse-Compton components as required by the model.

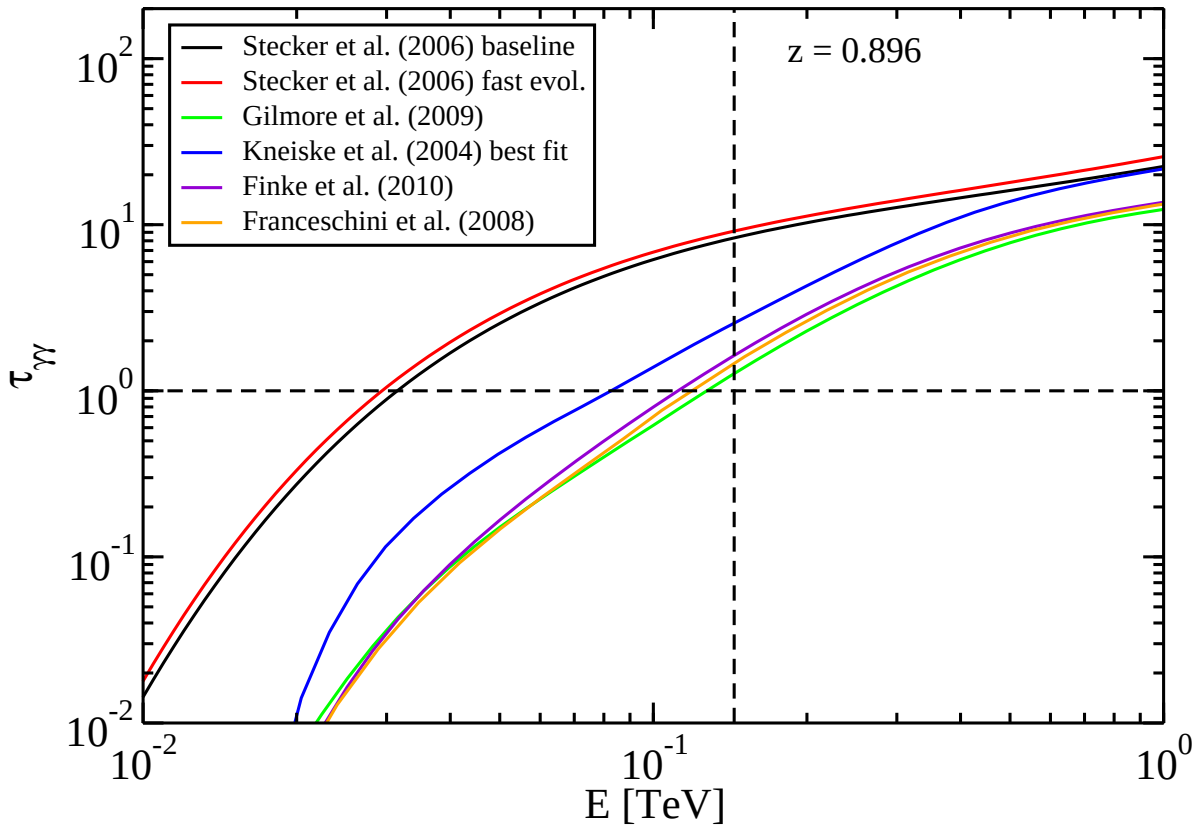

Fig. 5.— The $\tau_{\gamma\gamma}$ opacity versus energy for several EBL models at $z = 0.896$. The highest-energy photon of 145 GeV (rest frame energy = 275 GeV) within the 95% containment radius of the 4C +55.17 position is also indicated (vertical dashed line). The horizontal line simply denotes $\tau_{\gamma\gamma} = 1$. At the observed energy, attenuation from the EBL is expected even for those models which predict low levels of EBL.

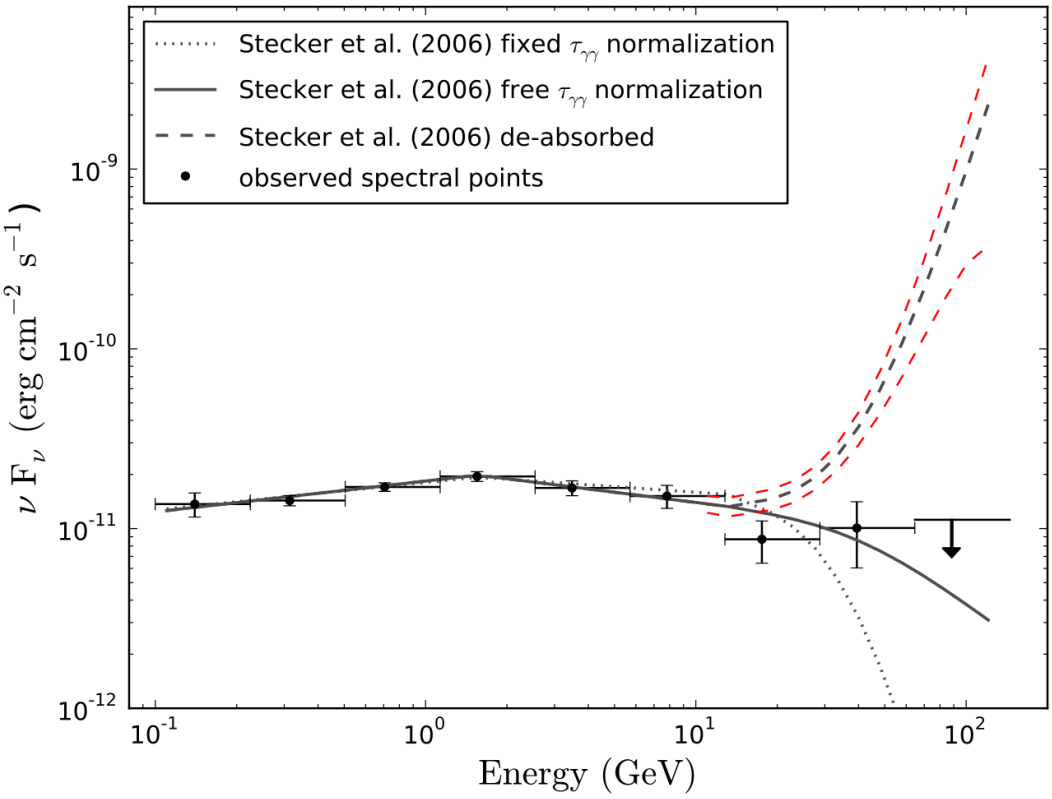

Fig. 6.— The de-absorbed spectrum of 4C +55.17 (thick dashed line, gray) along with 1σ error bars (thin dashed lines, red) using the Stecker et al. (2006) baseline model. Observed spectral points without de-absorption, along with the observed spectrum with $\tau_{\gamma\gamma}$ normalization left free (solid line) and fixed to 1 (dotted line), are plotted for comparison. The de-absorbed spectrum shows the non-physical behavior of an unbounded exponential rise up to the observed LAT energy of 145 GeV. This trend, which is preferred by 3.9σ over a single power law, increases the intrinsic spectrum by two orders of magnitude above the observed inverse Compton peak and requires the modeling of an additional (and unknown) spectral component (see Figures 3 and 4).

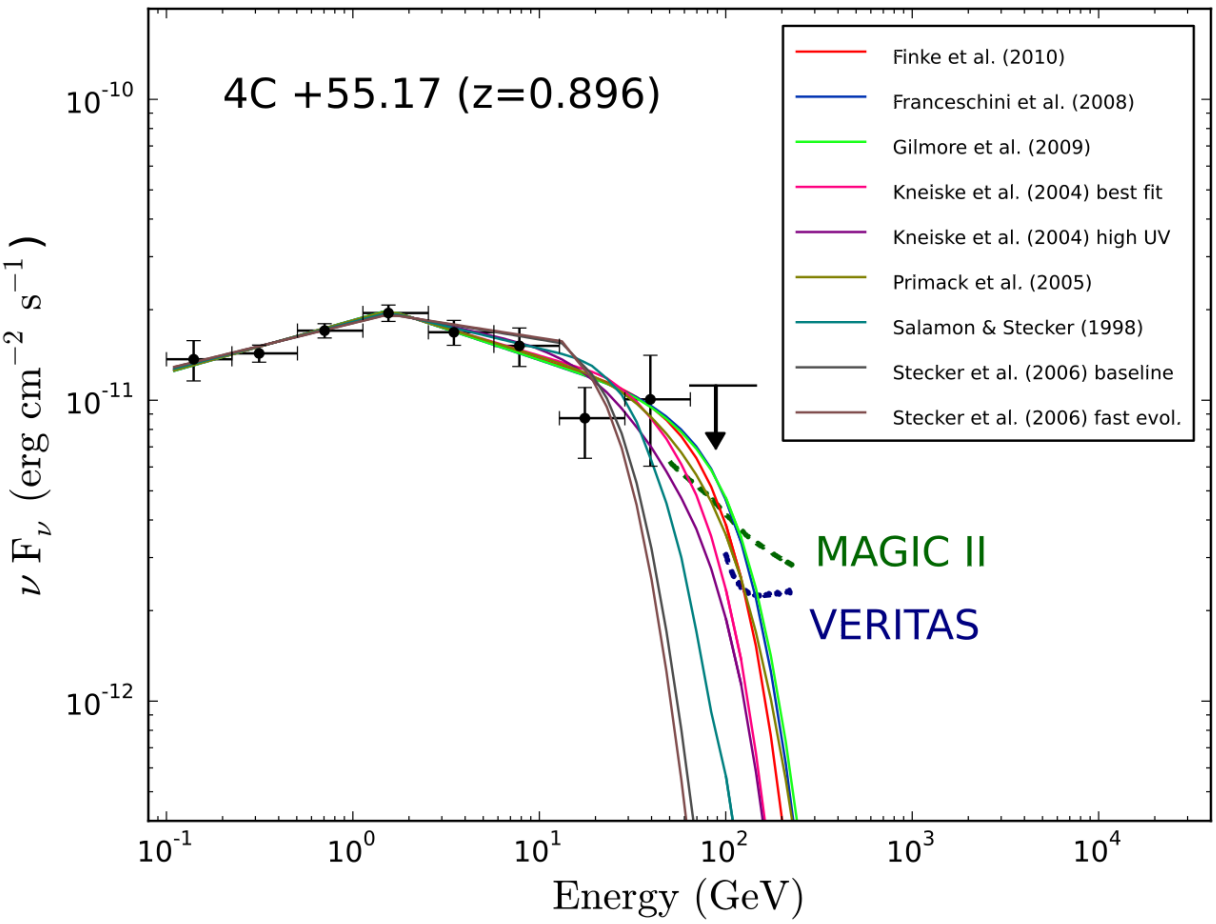

Fig. 7.— The observed LAT spectrum fit to a broken power law with attenuation from 9 different EBL models. The spectra are extrapolated beyond the observed energy of 145 GeV and compared against the MAGIC II and VERITAS differential flux sensitivity curves for a 50 hour, 5σ detection of a source characterized by an exponentially decreasing spectrum (see Appendix B). For several EBL models, the 4C +55.17 spectrum is found to intercept with both the VERITAS and MAGIC II sensitivities, making 4C +55.17 a viable candidate for future ground-based VHE observations.